Eur. Phys. J. D (2021) 75:306
https://doi.org/10.1140/epjd/s10053-021-00318-x

THE EUROPEAN PHYSICAL JOURNAL D

Regular Article – Atomic and Molecular Collisions

Electron collisions with formic acid

Pedro A. S. Randi[a], Giseli M. Moreira[b], and Márcio H. F. Bettega[c]

Departamento de Física, Universidade Federal do Paraná, Caixa Postal 19044, Curitiba, Paraná 81531-980, Brazil

Received 1 October 2021 / Accepted 30 November 2021 / Published online 15 December 2021

Abstract. We report elastic, electronically inelastic, total ionization and total cross sections for the scattering of electrons by *trans*-formic acid. The calculations of the elastic and electronically inelastic cross sections were performed with the Schwinger multichannel method implemented with norm-conserving pseudopotentials. The electronically inelastic calculations were done within the minimal orbital basis for single configuration interaction approach with different multichannel coupling schemes considering from 1 up to 51 open channels, which enable us to study the influence of the multichannel coupling effects on the calculated cross sections. Polarization effects in the elastic channel were taken into account considering only the excitations related to the pairs used in the minimal orbital basis for single configuration interaction approach. We found that the magnitude of the elastic and inelastic cross sections decreases as more channels are treated as open in the scattering calculations. The calculated elastic differential cross sections present an overall good agreement with previous studies found in the literature. The elastic integral cross section presents a well-known π^* shape resonance centered at 1.96 eV. The total ionization cross section was calculated with the binary-encounter-Bethe model and presents a good agreement with previous results from the literature. The total cross section was estimated using the calculated elastic, inelastic and ionization cross sections.

1 Introduction

To develop accurate mathematical models of the biological and interstellar medium it is important to understand precisely how the interactions between low-energy electrons (LEEs) and molecules occur. In the early 2000s, Boudaïffa et al. [1] showed that LEEs could damage the genetic material through single- and double-strand breaks of the DNA molecules. The main mechanism responsible for this damage is known as dissociative electron attachment (DEA), which is mediated by the capture of the incident electron by an unoccupied molecular orbital of one of the DNA bases, forming a transient negative ion (also called resonance). This resonance, in turn, may lead to molecular dissociation, damaging the DNA structure [2,3]. LEEs also play an important role in astrochemistry [4]. They are produced in vast quantities on the interstellar medium through the interaction between high energy radiation (viz., cosmic rays, γ rays, x-rays, high energy electrons and ions) and matter. These LEEs may play a fundamental role in the synthesis of complex organic molecules and may be related to the origin of life itself [5].

Formic acid (HCOOH - ball and stick model shown in Fig. 1) is the simplest organic acid and an important building block for complex organic molecules. For that matter, it has been used as a prototype to study more complex organic systems [6]. Asides from that, it is also an important precursor molecule in organic synthesis observed in the interstellar medium in chondritic meteorites [7], the coma of comet C/1995 O1 (Hale-Bopp) [8], hot molecular cores [9], interstellar ices [10] and in Galactic centers [11].

Many studies regarding the interaction between LEEs and formic acid have been published in recent years. The DEA of formic acid was studied experimentally by Pelc et al. [13] and by Prabhudesai et al. [14] and its dissociation mechanism has been studied theoretically extensively [15–18]. Experimentally, Allan [19] measured absolute differential elastic and vibrational excitation cross section for formic acid at 135°, finding a π^* shape resonance around 2.0 eV. Vizcaino et al. [20] measured elastic absolute-differential cross sections (DCSs) for formic acid for the incident electron energies of 1.8, 5, 10, 15, 20, 30, 40 and 50 eV through a relative flow technique and calculated elastic integral cross section (ICS) and momentum-transfer cross section (MTCS) from the measured DCSs. Kimura et al. [21] measured the total cross section (TCS) for the scattering of LEEs by formic acid, finding a shape resonance around 1.8 eV. On the theoretical side, Gianturco and

[a] e-mail: pasr@fisica.ufpr.br
[b] e-mail: gmm08@fisica.ufpr.br (corresponding author)
[c] e-mail: bettega@fisica.ufpr.br

Lucchese [22] carried out some calculations and found two resonances centered at 3.48 eV and 12.26 eV of A'' and A' symmetries, respectively. In another work [23], the same authors calculated some elastic DCSs for the impact of electrons by the *trans* and *cis* isomers of formic acid using a single center expansion technique. Gianturco et al. [24] studied the electron interaction with the dimer of formic acid and also reported the ICS for the monomer species. Trevisan et al. [25] through the complex Kohn variational method calculated the elastic MTCS and DCSs for the scattering of electrons by formic acid for energies from 0.1 to 15 eV, finding a π^* shape resonance at 1.9 eV and evidences that support the presence of a virtual state. Bettega [26] calculated DCSs and MTCS with the Schwinger multichannel (SMC) method implemented with norm-conserving pseudopotentials (SMCPP) in the static-exchange (SE) and static-exchange plus polarization (SEP) approximations, finding the π^* shape resonance centered around 3.5 eV in the SE approximation and at around 1.9 eV in the SEP approximation. A good agreement was found between the calculated DCSs and the measurements from Vizcaino et al. [20] for low-impact energies. Vinodkumar et al. [27] reported total, total elastic and total ionization cross sections (TICS) calculated with the spherical complex optical potential formalism (SCOP) with the complex scattering potential-ionization contribution (CSP-ic) for energies above 15 eV. Vinodkumar et al. [28] calculated the TCS for the electron scattering by formic acid and formaldehyde with the R-matrix method and SCOP formalism for incident energies of 0.01 to 2 keV. In a recent work, Vinodkumar et al. [29] calculated the TICS of H_2S, PH_3, HCHO and HCOOH with the Improved Complex Scattering Potential-ionization contribution (ICSP-ic) formalism. Możejko [30], using the binary-encounter-Bethe (BEB) model and the 6-311G(d) basis set calculated the TICS for formic acid. Electron-impact ionization cross sections of formic acid were measured by two separate experiments performed by Zawadzki [31]. Pilling et al. [32] also measured the TICS for formic acid. To the best of our knowledge, the electronic excitation cross sections for the scattering of LEEs by formic acid were not available in the literature.

In this study, the elastic, electronically inelastic, total ionization and total cross sections for the electron-formic acid scattering are reported. The scattering amplitudes for the elastic and electronically inelastic cross section were calculated with the SMCPP method including up to 51 open channels. DCSs and ICS for the elastic channel and excitation from the ground state to the two lowest lying triplets ($1^3A'$ and $1^3A''$) and singlets ($1^1A'$ and $1^1A''$) states of formic acid are reported. The inclusion of multichannel-coupling effects in the scattering calculations improves the previous elastic scattering results obtained with the SMCPP method [26], specially at higher impact energies. The TICS was calculated with the BEB model. The calculated cross sections are compared with previous results reported in the literature [20,21,23–32], finding an overall good agreement.

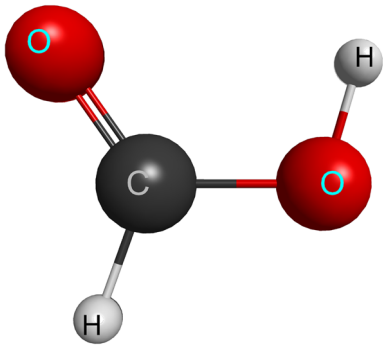

Fig. 1 Ball and stick model of formic acid (HCOOH) in its *trans* configuration. (Generated with MacMolPlt [12])

The description of electronic excitation of molecular targets by electron impact is a challenge both theoretically and experimentally. From the theoretical point of view, the cross section calculations for such process rely on the description of the electronic excited states and of a method that is capable of addressing such a collision problem. There are few ab-initio methods that allow these calculations, such as the R-matrix [33], the complex Kohn [34] and the Schwinger multichannel [35,36] methods. Other theoretical approaches make use of a complex potential to take the inelastic channels into account (in this case inelastic means all that is not elastic) [37,38]. In the earlier applications of the SMC method in electronic excitation calculations [39], the excited states were described considering just one hole-particle pair, using in the description of the target excited state the improved virtual orbitals (IVOs) [40]. The development of the minimal orbital basis for single configuration interaction (MOB-SCI) approach [41] allowed the use of a certain number of hole-particle pairs to describe a few chosen excited states, which are compatible with a full single configuration interaction calculation. However, the MOB-SCI approach still considers only single-excitations of the target. A recent methodology proposed by Falkowski, Lima and Kossoski [42], the truncated configuration interaction with single excitations (TCIS), allowed calculations including up to 431 open channels to be performed with the SMC method. In the case of the R-matrix and the complex Kohn methods the electronically excited states are described by other approaches, such as the complete active space configuration interaction (CASCI) [33,34] method. Although the description of the states included in the scattering calculations have come a long way from the initial IVOs description, it still presents a real challenge to theoreticians and an important aspect of the scattering calculations that can be improved.

The remainder of this manuscript is organized as follows. In Sect. 2 a brief discussion of the methods that have been used is presented and in Sect. 3 the computational details used will be presented. After that, in Sect. 4, the results and discussions are presented

and, finally, in Sect. 5, a brief summary of our results is given.

2 Theory

The elastic and electronically inelastic cross sections were obtained with the SMC method, which is an extension of the Schwinger variational principle for the scattering amplitude and was developed by Kazuo Takatsuka and Vincent McKoy [35,36] in the early 80's at the California Institute of Technology. Since its first implementation, the SMC method is capable of addressing some important aspects of the electron-molecule collision problem such as elastic [43] and electronically inelastic [44] channels, molecular targets of arbitrary geometry [43], and the inclusion of the exchange [43] and polarization [45] interactions, which are computed in an ab-initio way.

Here, we use the most recent implementation of the SMC method, in which the nuclei and the core electrons of each atom of the target are represented by a norm-conserving pseudopotentials, and the SMC code runs with parallel processing. Since these implementations have been recently described elsewhere [46], here we will only give a brief description of the method highlighting the key aspects relevant to this work. The computational details, such as the basis set used and the procedure to describe the target bound states, will be given in Sect. 3.

In the SMC method, the scattering amplitude is given by:

$$f(\mathbf{k}_f,\mathbf{k}_i) = -\frac{1}{2\pi}\sum_{m,n}\langle S_{\mathbf{k}_f}|V|\chi_m\rangle(d^{-1})_{mn}\langle\chi_n|V|S_{\mathbf{k}_i}\rangle, \tag{1}$$

where:

$$d_{mn} = \langle\chi_m|A^{(+)}|\chi_n\rangle, \tag{2}$$

and:

$$A^{(+)} = \frac{\hat{H}}{N+1} - \frac{(P\hat{H}+\hat{H}P)}{2} + \frac{(PV+VP)}{2} - VG_P^{(+)}V. \tag{3}$$

In the equations above, V is the interaction potential between the incident electron and the target and $\hat{H} = E - H$ is the total energy of the collision minus the full Hamiltonian $H = H_0 + V$. P is a projector on the open channel space defined as

$$P = \sum_{\ell=1}^{N_{open}} |\Phi_\ell\rangle\langle\Phi_\ell|, \tag{4}$$

where $|\Phi_\ell\rangle$ is the ground state (if $\ell = 1$) or an electronically excited state of the N-electron molecular target described with a single-excitation configuration interaction technique where the states are expanded in a set of singly excited spin-adapted Slater determinants $|\Phi_m^s\rangle$, and N_{open} is the number of open channels included in that level of calculation. $G_P^{(+)}$ is the free particle Green's function $G_0^{(+)}$ projected on the P-space. $|S_{\mathbf{k}_i,f}\rangle$ is the solution of the unperturbed Hamiltonian H_0 and is the product of a target state and a plane wave. $|\chi_m\rangle$ is a set of $(N+1)$-electron configuration-state functions (CSFs) used for the expansion of the trial scattering function. The CSFs are constructed as:

$$|\chi_{mn}\rangle = \mathcal{A}|\Phi_m^s\rangle \otimes |\varphi_n\rangle, \tag{5}$$

where $\mathcal{A}$ is the antisymmetrization operator of $N+1$ electrons, $|\Phi_m^s\rangle$ is the ground state of the molecule (if $m = 1$) described at the Hartree-Fock level, or $|\Phi_m^s\rangle \equiv (h_m \rightarrow p_m)^s$ is a singly-excited Slater determinant (if $m > 1$) representing the promotion of an electron from an occupied (hole, h_m) orbital to an unoccupied (particle, p_m) with spin s ($s = 0$ for singlets or $s = 1$ for triplet). $|\varphi_n\rangle$ is a scattering orbital represented by an unoccupied molecular orbital. The inclusion of the singly-excited states in the construction of the configuration space introduces the polarization effects (distortion of the molecular cloud) of the target due to the incident electron.

Since the SMC method uses only square integrable functions in the expansion of the scattering wave function, the long range dipole interactions is poorly described. To improve the elastic cross sections a Born-closure procedure [46] is employed. In summary, the low partial wave contributions obtained from the SMC method are retained until a certain l_{SMC} value and the higher partial wave contributions are obtained in the first Born approximation (FBA). The FBA scattering amplitude is obtained for the permanent dipole moment of the molecular target.

The total ionization cross section was obtained with the binary-encounter-Bethe [47] model. In this model, the ionization cross section from the ith molecular orbital is calculated by

$$\sigma_i(t_i) = \frac{4\pi a_0^2 N_i (R/B_i)^2}{t_i + u_i + 1} \times \left[\frac{ln(t_i)}{2}\left(1 - \frac{1}{t_i^2}\right) + 1 - \frac{1}{t_i} - \frac{ln(t_i)}{t_i+1}\right] \tag{6}$$

where, $t_i = E/B_i$, $u_i = U_i/B_i$, E is the energy of the incident electron, a_0 is the Bohr radius, R is the Rydberg energy, N_i is the occupation number of the ionizing orbital, B_i is the bound state biding energy of the ionizing orbital and U_i is the orbitals' average kinetic energy. The total ionization cross section is obtained as

$$\sigma_{\mathrm{BEB}} = \sum_{i=1}^{N_{\mathrm{occ}}} N_i\sigma_i(t_i) \tag{7}$$

where N_{occ} is the number of occupied molecular orbitals of the target.

3 Computational details

The geometry of the molecular ground state was optimized in the C_s point group at the MP2/aug-cc-pVDZ level with the computational package GAMESS [48]. For the bound states and scattering calculations, we have replaced the core electrons of carbon and oxygen by the norm-conserving pseudopotentials of Bachelet, Hamann and Schlüter [49], and the valence electrons of these atoms were described with the basis set used in a previous calculation [26], containing $5s5p3d$ uncontracted Cartesian Gaussian (CG) functions, generated according to Bettega *et al.* [50]. Extra CG functions were included at the molecular center of mass [26]. The $4s/3s$ basis set of Dunning [51] with one additional p-type function with exponent 0.75 was used for the H atoms.

The elastic and electronically inelastic cross sections presented in this work were calculated within the MOB-SCI approach [41], which has recently been applied to produce reliable cross sections for many systems [52]. In this strategy, the target states that compose the open-channel space are expanded on a basis of a minimal number of singly-excited spin-adapted Slater determinants $|\Phi_m^s\rangle$ that can reproduce as closely as possible the first few electronically excited states obtained with a full single configuration interaction (FSCI) calculation. In practice, the first step is to obtain a set of IVOs [40] to represent the unoccupied molecular orbitals of the target, then perform a FSCI calculation and, from that, select the determinants that are most relevant to the description of the electronically excited states of interest.

Here, the IVOs were generated using triplet coupling with the hole made in the highest occupied molecular orbital (HOMO) and the FSCI calculation included 1269 single electronic excitations (hole-particle) producing 2538 electronic excited states (1269 singlets and 1269 triplets). From these 1269 pairs, 25 were selected to perform the MOB-SCI calculation with the aim of describing well the first 20 electronically excited states obtained with the FSCI calculation. This procedure produced a total of 50 excited electronic states (25 singlets and 25 triplets), from which 20 are considered physical states while the remaining states are considered pseudostates. The vertical excitation energy of the first 20 states obtained with the FSCI and MOB-SCI calculations are presented in Table 1. The MOB-SCI calculation can reproduce well the results obtained with the FSCI calculation for the first few excited states and present a fair agreement with the results of the CASCI [28], couple cluster with singles and doubles (CCSD) [53], two-configuration electron-hole potential (TCEHP) [54] and the frozen core single excitation configuration mixing (FCSCM) [55] calculations and the electron energy-loss spectra (EELS) [56,57] found in the literature. The vertical excitation energies of the 50 electronically excited states obtained with the MOB-SCI calculation (along the with the thresholds for the scattering calculations) are summarized in Fig. 2.

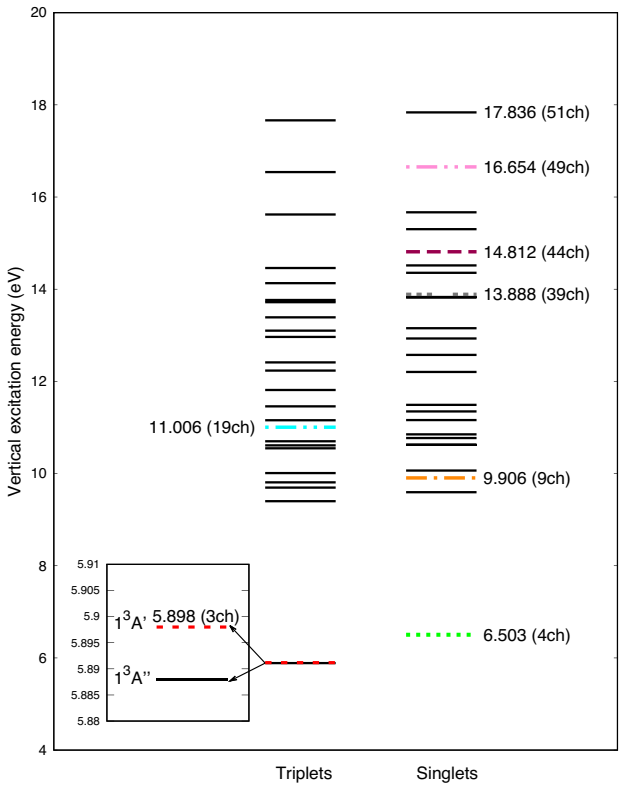

Fig. 2 Schematic representation of the vertical excitation energies (in eV) of the 50 electronically excited states of formic acid obtained with the MOB-SCI calculation. The dashed red line correspond to the threshold of the 3ch scattering calculation; the small-dashed green line, 4ch; long-dash-dot orange line, 9ch; dot-dot-dashed cyan line, 19ch; dot-dot-dot grey line, 39ch; dashed brown line, 44ch; dot-dash pink line, 49ch. We also indicate the 51ch threshold

For the scattering calculations performed with the SMCPP method, the hole-particle pairs used to obtain the set of determinants $|\Phi_m^s\rangle$ included in the construction of the CSFs (equation 5) are the same 25 pairs used in the MOB-SCI calculation plus the ground state, while all 141 unoccupied IVOs are used as scattering orbitals ($|\varphi_n\rangle$). The same set of singly excited spin-adapted Slater determinants $|\Phi_m^s\rangle$ used in the expansion of the target wave function is used in the construction of the CSFs, giving rise to 1772 CSFs of A' symmetry and 1894 CSFs of A'' symmetry. Contrary to most of the previous calculations done with the SMCPP method [52], closed channels were not included in the construction of configuration space, that is, virtual excitations were not added to the set o spin-adapted Slater determinants used in the construction of the CSFs. As a consequence the polarization effects are described only by the 3666 CSFs obtained from the set of spin-adapted Slater determinants $|\Phi_m^s\rangle$ used in the MOB-SCI calculation.

Table 1 Vertical excitation energies (in eV) of the first 20 excited electronic states obtained from a full single configuration interaction (FSCI) and from a minimal orbital basis for single configuration interaction (MOB-SCI) calculations

State	FSCI	MOB-SCI	Ref. [28]	Ref. [53]	Ref. [54]	Ref. [55]	Ref. [56]	Ref. [57]
$1^3A'$	5.651	5.898	7.30		4.85	4.80		
$1^3A''$	5.708	5.888	6.26		5.12	4.60		
$1^1A''$	6.408	6.503	6.57	5.86	5.83	5.24	5.8	5.7
$1^1A'$	9.201	9.595	9.88	7.82	9.84	8.14	8.4	8.4
$2^3A'$	9.231	9.402	10.38			7.98		
$2^3A''$	9.263	9.696	10.29			8.36		
$3^3A''$	9.392	9.809				8.72		
$2^1A''$	9.645	9.906	10.82	8.67		8.67	7.7	
$2^1A'$	9.707	10.066		8.42		8.70	8.9	
$3^3A'$	9.748	10.011				8.61		
$3^1A'$	10.189	10.623		8.61		9.16	10.1	
$4^3A'$	10.305	10.549				9.17		
$5^3A'$	10.368	11.006				9.42		
$3^1A''$	10.424	10.624				9.15	10.1	
$4^3A''$	10.524	10.612				9.14		
$5^3A''$	10.572	10.701				9.59		
$4^1A''$	10.608	10.771				9.39		
$5^1A''$	10.663	10.851				9.70		
$4^1A'$	10.751	11.162				9.64		
$6^3A''$	10.946	11.157				9.82		

These results are compared to the theoretical calculations from Vinodkumar et al. [28] (CASCI), Osted et al. [53] (CCSD), Iwata and Morokuma [54] (TCEHP), Demoulin [55] (FCSCM) and experimental measurements of Ari and Güven [56] (EELS) and Fridh [57] (EELS)

The open-channel space for the elastic and electronically inelastic scattering calculations performed with the SMCPP method is composed of the elastic channel and the 50 electronic excited states obtained according to the MOB-SCI strategy, i.e, these 51 channels are, if energetically accessible, allowed to the molecular target during the collision process. In this work, we will adopt the nomenclature N_{open}ch to describe the different levels of calculations, where N_{open} is the number of channels considered open in that level of approximation. For example, 1ch is a calculation where only the elastic channel is treated as open, 3ch is a calculation where the elastic, the first and second electronically inelastic channels are accessible, 25ch is a calculation where the elastic and first 24 electronically inelastic channels are treated as open and so on. With this in mind, the change in the N_{open} value enables us to study how different multichannel-coupling schemes affect the magnitude and behaviour of the cross sections. The scattering calculations were performed with N_{open} equal to 1, 3, 4, 9, 19, 39, 44, 49 and 51. The energies thresholds for each of these scattering calculations are summarized in Fig. 2.

The present value of the calculated permanent dipole moment of *trans*-formic acid is 1.73 D, in good agreement with the values of 1.71 D calculated by Bettega [26] and 1.72 D calculated by Trevisan et al. [25], overestimating the result of 1.45 D of Vinodkumar et al. [28] and the experimental result of 1.41 D [58]. The l_{SMC} values used in this work are presented in Table 2 and are choose so as the DCS obtained with the SMC and FBA agrees well for angles above 30 degrees in each energy regime.

Table 2 l_{SMC} Chosen for the Born-Closure Procedure performed in the calculations of the elastic cross sections

l_{SMC}	Energies
1	1.0 to 1.2
2	1.3 to 1.8
3	1.9 to 2.5
4	3.0 to 5.0
5	5.5
6	6.0 to 7.5
7	8.0 to 12.0
8	13.0 to 14.0
9	15.0 to 16.0
10	17.0 to 50.0

Energy ranges are presented in eV

The parameters used in the calculation of the TICS, i.e., the parameters used in equation 6 were obtained with the computational package GAMESS [48] employing the aug-cc-pVDZ basis set for the ground state of formic acid. The calculated ionization potential is 12.88 eV, overestimating the values of 11.33 eV [27,29] and 11.46 eV [30] found in the literature. It is important to note that this calculation was performed apart from the calculations of the elastic and electronically inelastic cross sections, meaning that the ionization channel does not compete for the flux that

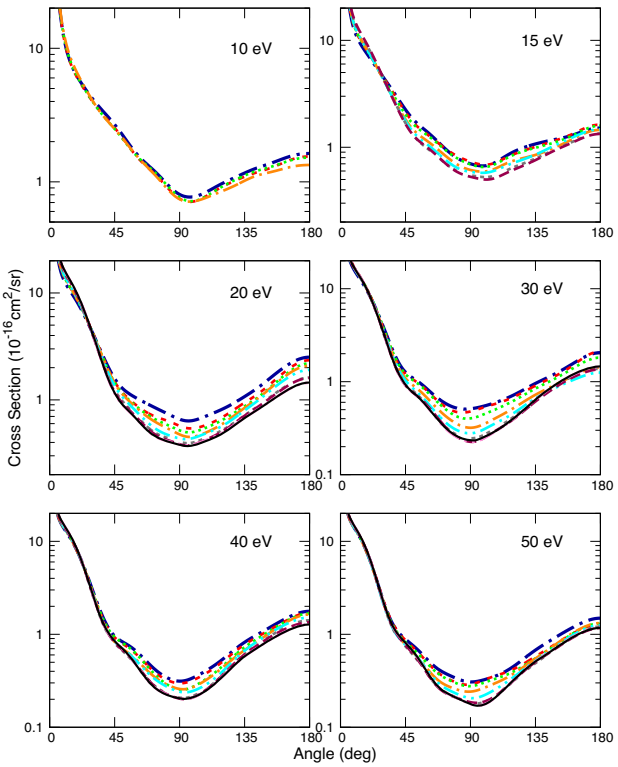

Fig. 3 Present elastic differential cross sections for the impact energies of 10, 15, 20, 30, 40 and 50 eV with different channel coupling schemes. Dash-dot blue line, 1ch; dashed red line, 3ch; small-dashed green line, 4ch; long-dash-dot orange line, 9ch; dot-dot-dashed cyan line, 19ch; dot-dot-dot grey line, 39ch; dashed brown line, 44ch; dot-dash pink line, 49ch; full black line 51ch. As more channels are opened, the magnitude of the DCS decreases due to the multichannel coupling effect

defines the elastic and the electronically inelastic cross sections.

4 Results and discussion

4.1 Elastic channel

The elastic DCSs calculated with the SMCPP method and using the Born-closure procedure for the impact energies of 10, 15, 20, 30, 40 and 50 eV, with different multichannel coupling schemes, are presented in Fig. 3. The overall behavior of all elastic DCSs shown in Fig. 3 is similar, having a minimum around 90 degrees and a large forward scattering magnitude due to the long range dipole interaction between the target molecule and the incident electron.

The elastic DCSs presented in Fig. 3 follow the expected trend: the magnitude of the DCSs decreases as more channels are treated as open in the scattering calculations. This is a result of the competition among the accessible channels for the flux that defines the elastic cross section. The 1ch calculation has only the elastic channel open and all the flux defines only the elastic cross section. In the calculations where the molecule can be electronically excited ($N_{\text{open}} > 1$) the electronically inelastic channels compete for the flux that before only defined the elastic cross section, resulting in the decrease of the magnitude of the elastic cross section. This multichannel-coupling effect becomes more relevant as the impact energy increases, since more channels are energetically accessible at higher energies.

The comparison between the calculated elastic DCSs with only the elastic channel open (1ch) and the best multichannel-coupling scheme for each energy (9ch at 10 eV, 44ch at 15 eV and 51ch for energies above 15 eV) with the results from the literature [20,23,25,26] are presented in Figs. 4 and 5. The calculated cross sections present an overall good agreement with the results from the literature. The 1ch-DCS at 5 eV and the DCSs calculated with the best multichannel-coupling scheme at 10, 15, 20 and 30 eV underestimate the measurements from Vizcaino et al. [20] while at 40 and 50 eV our calculations show a good agreement with the experimental data. The 1ch results agree well with the results of Trevisan et al. [25] and the previous calculations performed by Bettega [26] at the 1ch-SEP (at 5, 10 and 15 eV) and 1ch-SE (at 20, 30, 40 and 50 eV) approximations and the small differences can be attributed to the different orbitals and polarization strategies used in the calculations. As expected, the calculations with the inclusion of the multichannel coupling underestimate the results from Bettega [26], especially at higher energies. The calculated DCSs with the best multichannel-coupling scheme show a good agreement with the calculated DCSs of Gianturco and Luchesse [23] for the forward scattering region for incident energies below 40 eV. This is expected since, according to the authors [23], their model does not account properly for the correlation-polarization effects in the intermediate and short-range distances that are important for the description of the backward scattering. At 40 and 50 eV the present DCSs overestimate their calculated DCSs. In the low-angle regions, the present DCSs show a small shoulder which is an effect of the Born closure procedure.

The differences found between the calculated DCSs and the experimental data for energies below 40 eV are puzzling. Based on previous works using the SMCPP with the MOB-SCI approach [52] it is expected that the magnitude of the DCSs become lower as the number of open channels increases to a point where either a good quantitative agreement or a small overestimation of the experimental data is reached. Yet, the calculations presented here with the best multichannel-coupling scheme for energies below 40 eV underestimate the experimental data [20]. There are two main hypotheses that may explain these discrepancies. The first one is related to the limitation of the MOB-SCI approach to deal only with single excitations to describe the electronically excited states of the target. Excitations of higher order are necessary in order to better describe the higher lying excited electronic states and, therefore, improve the description of how these

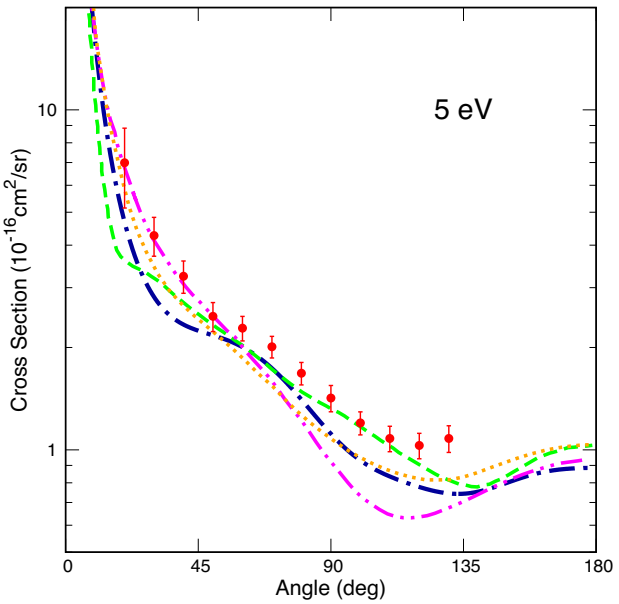

Fig. 4 Elastic differential cross sections for the impact energy of 5 eV. Dash-dot blue line, present 1ch calculation; dashed green line, results from Bettega [26]; dash-dot-dot magenta line, Gianturco and Lucchese [23]; dotted orange line, Trevisan et al. [25]; red circles, Vizcaino et al. [20]

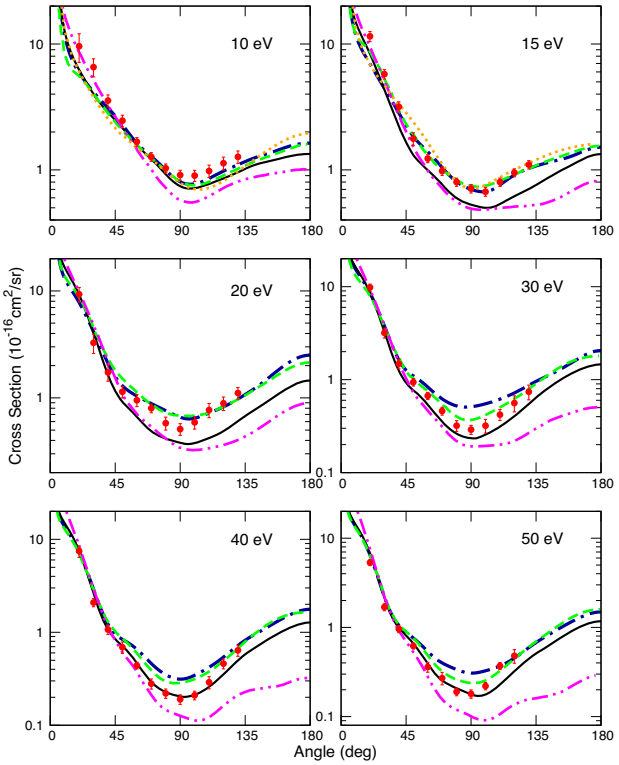

Fig. 5 Elastic differential cross sections for the impact energies of 10, 15, 20, 30, 40 and 50 eV. Dash-dot blue line, present 1ch calculation; full black line, present calculation with the best multichannel coupling scheme (9ch at 10 eV, 44ch at 15 eV and 51ch for energies above 15 eV); dashed green line, results from Bettega [26]; dash-dot-dot magenta line, Gianturco and Lucchese [23]; dotted orange line, Trevisan et al. [25]; red circles, Vizcaino et al. [20]

states compete for the flux that defines these cross sections in the scattering calculations. The second hypothesis is associated with the experimental data [20]. As the authors discuss, the experiment is conducted at room temperature and, as a consequence, the formic acid beam contains approximately 20% of dimers. As a result, the measured DCSs may be overestimated relative to the DCSs of the monomer, highlighting the difference between measurement and the present calculations. At 40 and 50 eV the incident electron is fast and its interaction time with the molecule is short. Thus, it does not distinguish the dimers from the monomers present in the experimental gas. Therefore, the presence of dimers in the experimental gas does not influence the cross section at higher impact energies. This hypothesis would explain why the calculations performed here agree well with experiments at 40 and 50 eV and underestimate it at lower energies.

The ICS calculated using different levels of multichannel coupling is presented in the upper panel of Fig. 6. The same multichannel-coupling effects observed in the DCSs can be observed in the ICS: the magnitude of the ICS decreases as the number of open channels increases. The 1ch-ICS presents some structures at high impact energies associated with pseudoresonances which are related to channels that are energetically accessible but treated as closed in this level of approximation. As more channels are opened these spurious structures are washed out from the ICS, as can be seen by the smooth 51ch-ICS, where all accessible channels are treated as open and the cross section is structureless. This is expected and is a well-known characteristic of the SMCPP method. The calculated ICS has a high magnitude at low incident energies as a consequence of the permanent dipole moment of the target molecule.

In the lower panel of Fig. 6 we present the ICS where the best channel coupling scheme is used in each energy regime and results found in the literature [20,24]. A π^* shape resonance centered at 1.96 eV is present in the calculated ICS, in good agreement with the resonance positions found at 1.25 eV by Pelc et al. [13], at 2.0 eV by Allan [19], at 1.8 eV by Kimura et al. [21], at 1.9 eV by Trevisan et al. [25] and in the 1ch-SEP calculation at 1.9 eV by Bettega [26] but disagreeing with the calculation of Gianturco and Lucchese [22] and Gianturco et al. [24] that found the shape resonance around 3.5 eV. These discrepancies are expected since, according to the authors [22,24], their calculation lacks the treatment of the short-range exchange and correlation effects and, as a consequence, the position of the shape resonance is overestimated. The position of the resonance found by the calculation presented here also disagrees with the results found by Vinodkumar et al. [28], where the resonance was positioned around 3.5 eV. At energies above 10 eV all the results agree well both in shape and in magnitude.

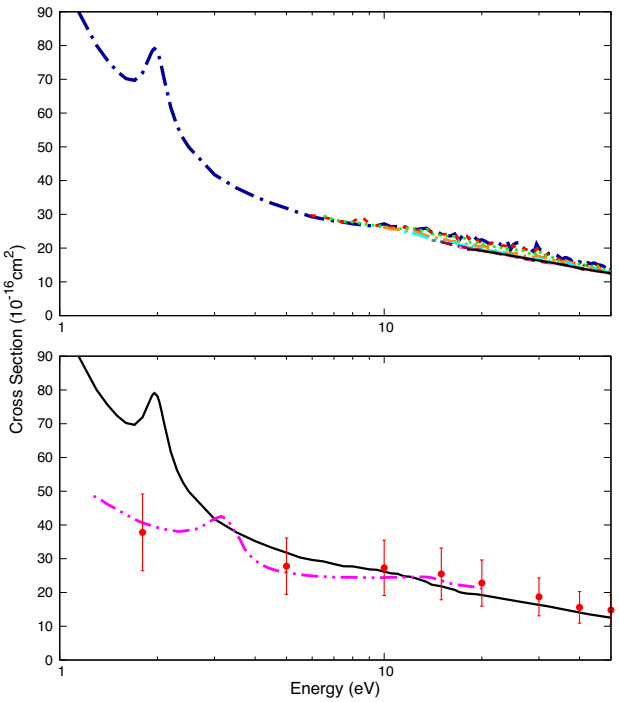

Fig. 6 Upper panel: ICS calculated with different multichannel coupling levels. Dash-dot blue line, 1ch; dashed red line, 3ch; small-dashed green line, 4ch; long-dash-dot orange line, 9ch; dot-dot-dashed cyan line, 19ch; dot-dot-dot grey line, 39ch; dashed brown line, 44ch; dot-dash pink line, 49ch; full black line 51ch. Lower panel: solid black line, present ICS with the best multichannel coupling; red circles, ICS measured by Vizcaino et al. [20]; dashed-dotted magenta line, ICS from Gianturco et al. [24]

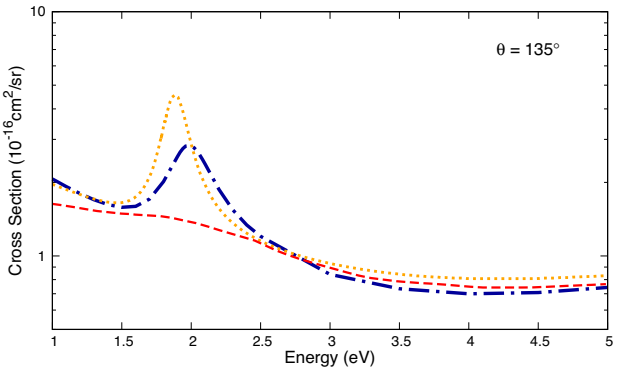

Fig. 7 Energy dependence of the elastic differential cross section at 135 degrees. Dash-dot blue line, present 1ch; Dashed red line, result from Allan [19]; dotted orange line, Trevisan et al. [25]

The energy dependence of the elastic DCS at 135 degrees for the impact energies from 1 to 5 eV is presented in Fig. 7. The cross section presents the well-known π^* resonance and an overall good agreement with the measurements of Allan [19] and the calculation of Trevisan et al. [25].

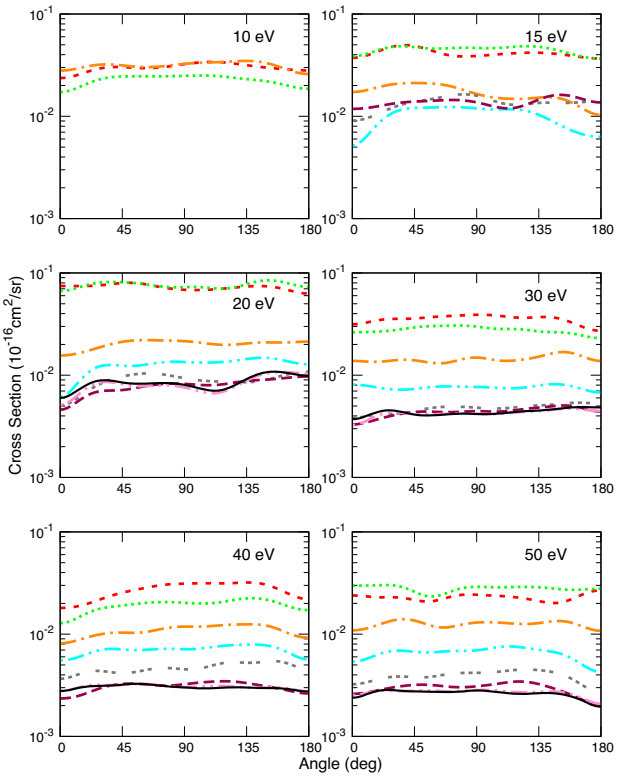

Fig. 8 Differential cross sections for the electronic excitation of the $1^3A''$ (5.888 eV) state of formic acid for the impact energies of 10, 15, 20, 30, 40 and 50 eV. Dashed red line, 3ch; small-dashed green line, 4ch; long-dash-dot orange line, 9ch; dot-dot-dashed cyan line, 19ch; dot-dot-dot grey line, 39ch; dashed brown line, 44ch; dot-dash pink line, 49ch; full black line 51ch

4.2 Excitation to triplet states

The DCSs for the electronic excitation of the $1^3A''$ (5.888 eV) and $1^3A'$ (5.898 eV) states of *trans*-formic acid calculated with different multichannel-coupling schemes are presented in Figs. 8 and 9, respectively. The DCSs for the electronic excitation of the $1^3A''$ are isotropic, while the DCSs for the electronic excitation of the $1^3A'$ are isotropic for energies below 30 eV. At 30, 40 and 50 eV a slightly higher backward scattering is observed.

The same trend observed in the elastic channel is observed for most of these excitation cross sections: the magnitude of the DCSs decreases as the number of open channels increases. The exceptions to this trend are the DCSs at 10 and 15 eV for the electronic excitation of the $1^3A''$ state (Fig. 8) and the DCS at 15 eV for the electronic excitation of the $1^3A'$ state (Fig. 9), where in some cases the calculated DCS with the less opened channels have a lower magnitude than one calculated with more open channels.

The electronically inelastic ICSs for the excitation from the ground state to the $1^3A''$ (5.888 eV) and $1^3A'$ (5.898 eV) states of formic acid calculated with the multichannel coupling schemes that better describe the

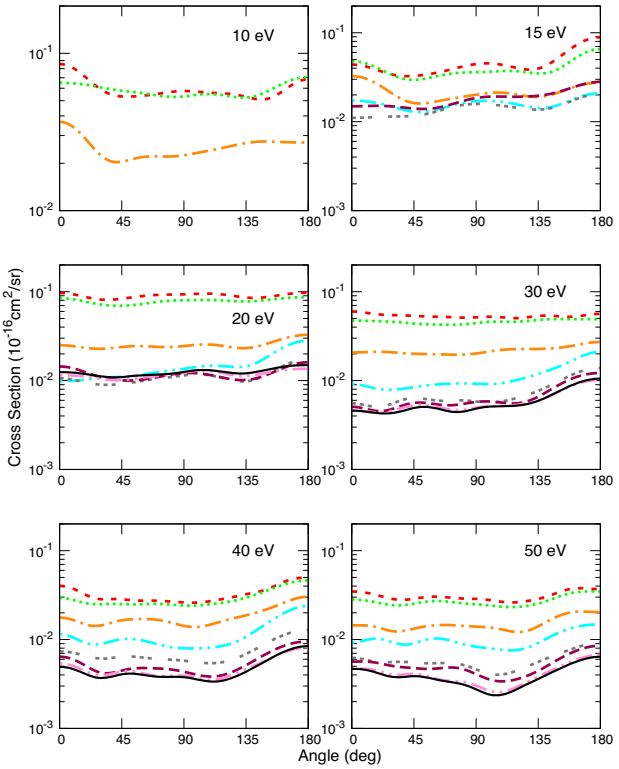

Fig. 9 Differential cross sections for the electronic excitation of the $1^3A'$ (5.898 eV) state of formic acid for the impact energies of 10, 15, 20, 30, 40 and 50 eV. Dashed red line, 3ch; small-dashed green line, 4ch; long-dash-dot orange line, 9ch; dot-dot-dashed cyan line, 19ch; dot-dot-dot grey line, 39ch; dashed brown line, 44ch; dot-dash pink line, 49ch; full black line 51ch

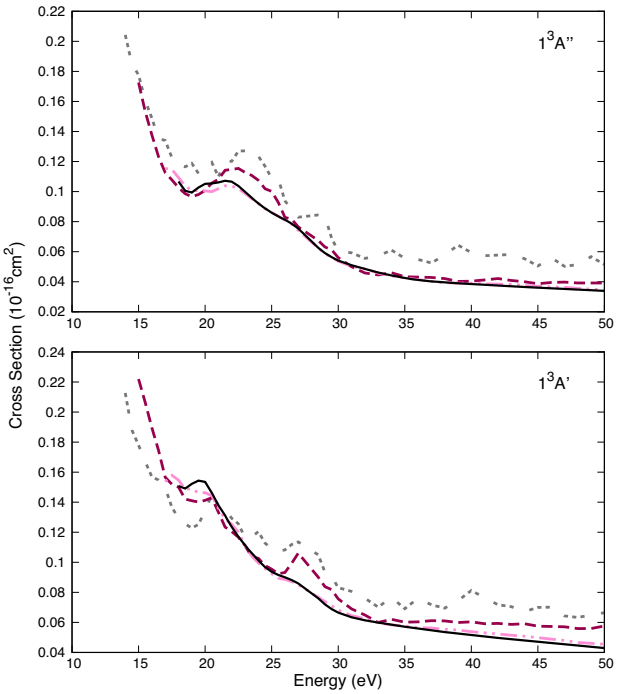

Fig. 10 Upper panel: Integral cross sections for the electronic excitation of the $1^3A''$ (5.888 eV) state of formic acid. Lower panel: Integral cross sections for the electronic excitation of the $1^3A'$ (5.898 eV) state of formic acid. Dot-dot-dot grey line, 39ch; dashed brown line, 44ch; dot-dash pink line, 49ch; full black line, 51ch

physics involved at this energy regime, i.e., with a high number of open channels, are presented in Fig. 10. The 39ch, 44ch and 49ch calculations present some spurious structures associated with the few channels that are energetically accessible but still treated as closed in this level of approximations, while the 51ch ICSs are structureless. The ICSs tend to decrease as the impact energy increases. Unfortunately, no electronic excitation cross sections were found in the literature for comparison.

4.3 Excitation to singlet states

The DCSs for the electronic excitation of the $1^1A''$ (6.503 eV) and $1^1A'$ (9.595 eV) states of *trans*-formic acid were calculated with different multichannel-coupling schemes (Figs. 11 and 12 , respectively). Once again, the multichannel-coupling effect is observed, since the magnitude of the DCSs decreases as the number of open channels in the scattering calculations increases.

The DCSs reported for the electronic excitation of the $1^1A''$ state (Fig. 11) are isotropic. The DCSs for the electronic excitation of the $1^1A'$ state (Fig. 12) are isotropic for low multichannel-coupling schemes and low-impact energies while at higher impact energies a minimum around 90 degrees is observed in the DCSs, favoring the backward and forward scattering. It is worth noting that the electronic transitions from the ground state to the $1^1A''$ and $1^1A'$ states are dipole-allowed. As a consequence, the long range dipole interaction plays an important role in the scattering process, especially for low scattering angles. Here, the Born-closure procedure was not performed and therefore it is expected that the DCSs shown in Figs. 11 and 12 are underestimating the scattering at low angles (below 30 degrees).

In Fig. 13 we present the electronically inelastic ICSs for the excitation from the ground state to the $1^1A''$ (6.503 eV) and $1^1A'$ (9.595 eV) states of formic acid. As is the case for the others ICSs shown in Figs. 6 and 10, when there is small number of open channels the remaining closed channels produce pseudoresonances which are washed out when all channels are treated as open (51ch).

4.4 Ionization cross section

The TICS calculated with the BEB method from threshold up to 2000 eV along with the results from Vinodkumar et al. [27], Vinodkumar et al. [29], Możejko [30], Zawadzki [31] and Pilling et al. [32] are presented in Fig. 14. An overall good agreement with the previous

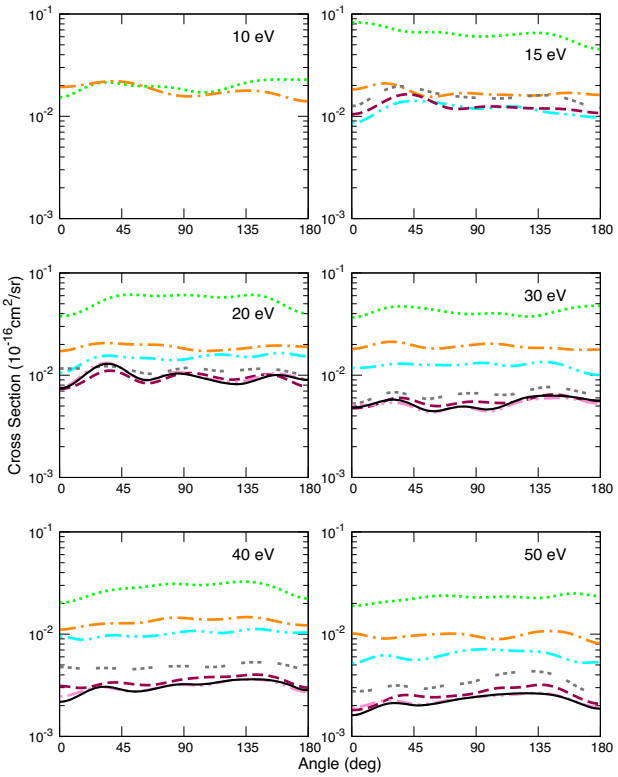

Fig. 11 Differential cross sections for the electronic excitation of the $1^1A''$ (6.503 eV) state of formic acid for the impact energies of 10, 15, 20, 30, 40 and 50 eV. Small-dashed green line, 4ch; long-dash-dot orange line, 9ch; dot-dot-dashed cyan line, 19ch; dot-dot-dot grey line, 39ch; dashed brown line, 44ch; dot-dash pink line, 49ch; full black line 51ch

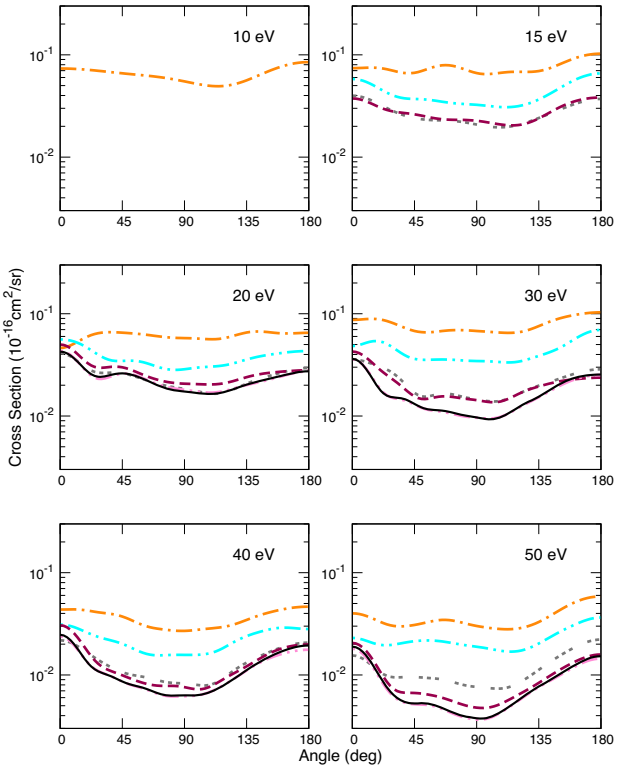

Fig. 12 Differential cross sections for the electronic excitation of the $1^1A'$ (9.595 eV) state of formic acid for the impact energies of 10, 15, 20, 30, 40 and 50 eV.Long-dash-dot orange line, 9ch; dot-dot-dashed cyan line, 19ch; dot-dot-dot grey line, 39ch; dashed brown line, 44ch; dot-dash pink line, 49ch; full black line 51ch

results from the literature is found [27,29–32] and the differences between the present TCIS and previous theoretical results are a consequence of different methods and input parameters used in the different calculations [27,29,30].

4.5 Total cross section

The TCS calculated as the sum of the elastic ICS (Fig. 6), the TICS (Fig. 14) and all the electronically inelastic cross sections is presented in Fig. 15. The TCS presents the well-known π^* shape resonance around 1.96 eV, increases at low incident energies due to the long-ranged dipole interactions between the incident electron and the target molecule and presents some spurious structures in the energy regime from 7 to 17 eV associated with threshold effects. The behavior of the present TCS is similar to the ICS, and agrees well with the calculations of Vinodkumar et al. [28] (except for the resonance position) and with the experimental data of Kimura et al. [21] for higher impact energies.

5 Summary

The elastic and electronically inelastic DCSs were calculated with the SMCPP method within the MOB-SCI approach with up to 51 open channels for the impact energies of 5, 10, 15, 20, 30, 40 and 50 eV. The magnitude of the DCSs decrease as the number of open channels increases due to the multichannel-coupling effects. The elastic DCSs are in good agreement with the results from the literature [20,23,25,26]. They present a minimum around 90 degrees and a high magnitude in the low-angle region due to the dipole interactions between the molecule and the incident electron. Although the inclusion of the multichannel-coupling effects in the scattering calculations improve the agreement with the experimental data [20], the calculated DCSs underestimates the measurements at the impact energies of 10, 15, 20 and 30 eV. We believe that in order to further improve the calculations, the description of the molecular target in the scattering calculations would have to go beyond the single configuration interaction approximation.

The elastic ICS presents a π^* shape resonance centered at 1.96 eV, in good agreement with some results found in the literature [13,19,21,25,26], and in disagreement with the results that place the resonance

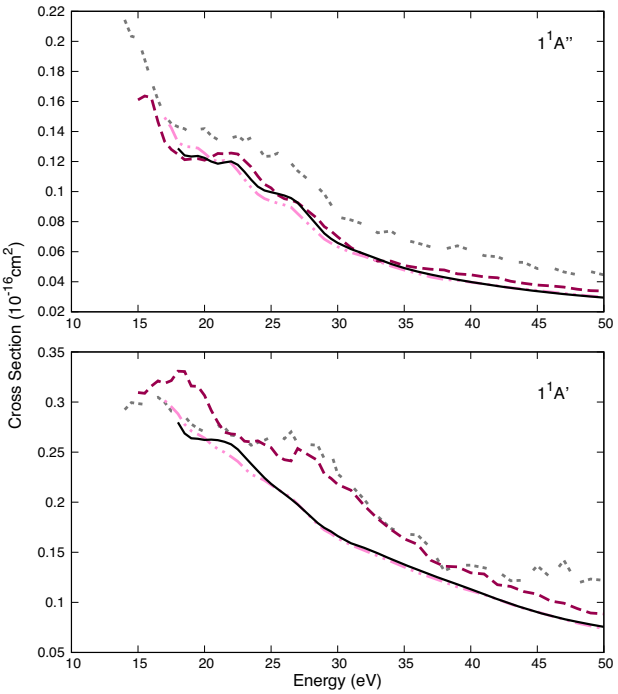

Fig. 13 Upper panel: Integral cross sections for the electronic excitation of the $1^1A''$ (6.503 eV) state of formic acid. Lower panel: Integral cross sections for the electronic excitation of the $1^1A'$ (9.595 eV) state of formic acid. Dot-dot-dot grey line, 39ch; dashed brown line, 44ch; dot-dash pink line, 49ch; full black line, 51ch

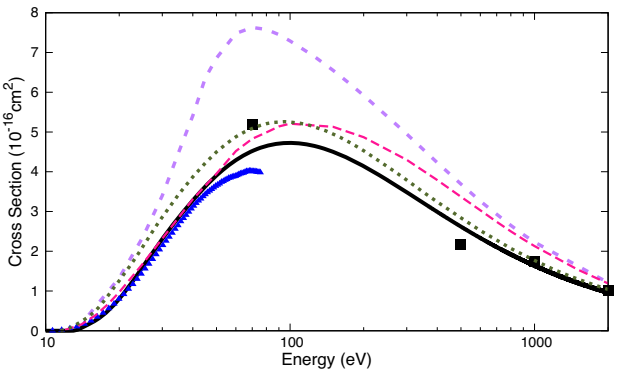

Fig. 14 Total ionization cross section for the scattering of low energy electrons by formic acid. Solid black line, present results; dashed purple line, Vinodkumar et al. [27]; dashed red line, Vinodkumar et al. [29]; dotted olive line, Możejko [30]; Blue triangles, Zawadzki [31]; Black squares, Pilling [32]

around 3.5 eV [22,24,28]. Another interesting feature that can be observed in our calculations is that the pseudoresonances in the high energy region of the 1ch-ICS are washed out as more channels are treated as open, to a point where the 51ch-ICS is structureless.

The electronically inelastic DCSs and ICSs for the excitation from the ground state to the $1^3A'$, $1^3A''$, $1^1A'$ and $1^1A''$ states of *trans*-formic acid were reported.

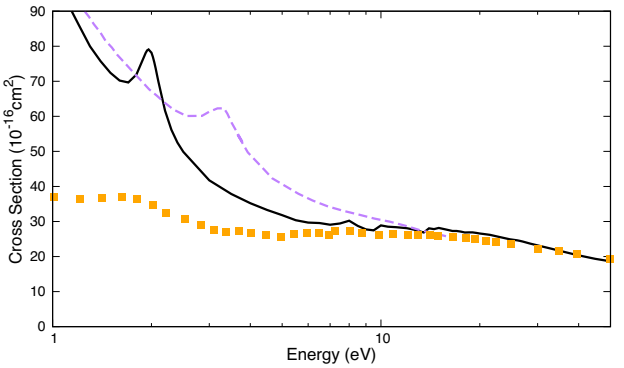

Fig. 15 Total cross section for the scattering of low energy electrons by formic acid. Solid black line, present results; dashed purple line, Vinodkumar et al. [28]; Yellow squares, Kimura et al. [21]

Unfortunately, no data regarding the electronic excitation of formic acid were found in the literature for comparison. More work regarding the electronic excitation of formic acid by electron impact is needed. The total ionization cross section was reported. The calculations performed with the BEB method and the aug-cc-pVDZ basis set have a overall good agreement with previous results from the literature [27,29–32]. The TCS, which is similar to the ICS, is also reported.

Acknowledgements P.A.S.R. and M.H.F.B. acknowledge the support from Conselho Nacional de Desenvolvimento Científico e Tecnológico (CNPq). M.H.F.B. acknowledges the Brazilian Agency Coordenação de Aperfeiçoamento de Pessoal de Nível Superior (CAPES) under CAPES/PrInt programme. The authors acknowledge the computational support from Professor Carlos M. de Carvalho at LFTC-DFis-UFPR and from CENAPAD-SP. The authors would like to thank Prof. Romarly F. da Costa, Prof. Marco A. P. Lima, Dr. Fábris Kossoski and MSc. Alan G. Falkowski for insightful discussion on MOB-SCI and on TCIS approaches. Professor Vincent McKoy had a profound influence in the research of electron-molecule collisions in Brazil. "Vince" will always be remembered as a wise mentor, an insightful collaborator and, above all, as a very dear friend.

Author contributions

PASR and GMM performed electron-scattering cross section calculations. All authors contributed in the analysis and discussion of the results and also in paper writing and proof reading.

Data Availability Statement This manuscript has no associated data in a data repository. [Authors' comment: All relevant data regarding this work is presented in the paper itself. The tabulated cross sections are available under request].

References

1. B. Boudaïffa, P. Cloutier, D. Hunting, M.A. Huels, L. Sanche, Science **287**, 1658 (2000)
2. M.A. Huels, I. Hahndorf, E. Illenberger, L. Sanche, J. Chem. Phys. **108**, 1309 (1998)
3. L. Sanche, Nature **461**, 7262 (2009)
4. M.C. Boyer, N. Rivas, A.A. Tran, C.A. Verish, C.R. Arumainayagam, Surf. Sci. **652**, 26 (2016)
5. S. Pilling, D.P.P. Andrade, A.C. Neto, R. Rittner, A.N. de Brito, J. Phys. Chem. A **113**, 11161 (2009)
6. G.A. Kumar, Y. Pan, C.J. Smallwood, M.A. McAllister, J. Comp. Chem. **19**, 1347 (1998)
7. J.F. Briscoe, C.B. Moore, Meteoritics. **28**, 330 (1993)
8. D. Bockéele-Morvan, D.C. Lis, J.E. Wink, D. Despois, J. Crovisier, R. Bachiller, D.J. Benford, N. Biver, P. Colom, J.K. Davies, E. Gérar, B. Germain, M. Houde, D. Mehringer, R. Moreno, G. Paubert, T.G. Phillips, H. Rauer, Astron. Astrophys. **353**, 1101 (2000)
9. S.-Y. Liu, D.M. Mehringer, L.E. Snyder, Astro. J. **552**, 654 (2001)
10. J.V. Keane, A.G.G.M. Tielens, A.C.A. Boogert, W.A. Schutte, D.C.B. Whittet, Astron. Astrophys. **376**, 254 (2001)
11. M.A. Requena-Torres, J. Martín-Pintado, A. Rodríguez-Franco, S. Martín, N.J. Rodríguez-Fernández, P. de Vicente, Astron. Astrophys. **455**, 971 (2006)
12. B.M. Bode, M.S. Gordon, J. Mol. Graph. Model. **16**, 133 (1998)
13. A. Pelc, W. Sailer, P. Scheier, M. Probst, N.J. Manson, E. Illenberger, T.D. Märk, Chem. Phys. Lett. **361**, 277 (2002)
14. V.S. Prabhudesai, D. Nandi, A.H. Kelkar, R. Parajuli, E. Krishnakumar, Chem. Phys. Lett. **405**, 172 (2005)
15. T.N. Rescigno, C.S. Trevisan, A.E. Orel, Phys. Rev. Lett. **96**, 213201 (2006)
16. G.A. Gallup, P.D. Burrow, I.I. Fabrikant, Phys. Rev. A **79**(4), 042701 (2009)
17. T.N. Rescigno, C.S. Trevisan, A.E. Orel, Phys. Rev. A **80**, 046701 (2009)
18. G.A. Gallup, P.D. Burrow, I.I. Fabrikant, Phys. Rev. A **80**(4), 046702 (2009)
19. M. Allan, J. Phys. B: At. Mol. Opt. Phys. **39**, 2939 (2006)
20. V. Vizcaino, M. Jelisavcic, J.P. Sullivan, S.J. Buckman, New J. Phys. **8**, 85 (2006)
21. M. Kimura, O. Sueoka, A. Hamada, Y. Itikawa, Adv. Chem. Phys. **111**, 537 (2000)
22. F.A. Gianturco, R.R. Lucchese, New J. Phys. **6**, 1 (2004)
23. F.A. Gianturco, R.R. Lucchese, Eur. Phys. J. D **39**, 399 (2006)
24. F.A. Gianturco, R.R. Lucchese, J. Langer, I. Martin, M. Stano, G. Karwasz, E. Illenberger, Eur. Phys. J. D **35**, 417 (2005)
25. C.S. Trevisan, A.E. Orel, T.N. Rescigno, Phys. Rev. A **74**, 042716 (2006)
26. M.H.F. Bettega, Phys. Rev. A **74**, 054701 (2006)
27. M. Vinodkumar, K.N. Joshipura, C. Limbachiya, N. Manson, Phys. Rev. A **74**, 022721 (2006)
28. M. Vinodkumar, H. Bhutadia, B. Antony, N. Manson, Phys. Rev. A **84**, 052701 (2011)
29. M. Vinodkumar, H. Bhutadia, C. Limbachiya, K.N. Joshipura, Int. J. Mass Spec. **308**, 35 (2011)
30. P. Możejko, Eur. Phys. J. Spec. Topics **144**, 233 (2007)
31. M. Zawadzki, Eur. Phys. J. D **72**, 12 (2018)
32. S. Pilling, A.C.F. Santos, W. Wolff, M.M. Sant'Anna, A.L.F. Barros, G.G.B. de Souza, N.V. de Castro Faria, H.M. Boechat-Roberty, Mon. Not. R. Astron. Soc. **372**, 1379–1388 (2006)
33. A. Loupas, K. Regeta, M. Allan, J.D. Gorfinkiel, J. Phys. Chem. A **122**, 1146 (2018)
34. T.N. Rescigno, A.E. Orel, Phys. Rev. A **88**, 012703 (2013)
35. K. Takatsuka, V. McKoy, Phys. Rev. A **24**, 2473 (1981)
36. K. Takatsuka, V. McKoy, Phys. Rev. A **30**, 1734 (1984)
37. G.L.C. de Souza, I. Iga, L.E. Machado, L.M. Brescansin, M.-T. Lee, J. Phys. B: At. Mol. Opt. Phys. **41**, 045203 (2008)
38. F. Blanco, L. Ellis-Gibbings, G. García, Chem. Phys. Lett. **645**, 71 (2016)
39. C. Winstead, Q. Sun, J.L.S. Lino, M.A.P. Lima, J. Chem. Phys. **98**, 2132 (1993)
40. W.J. Hunt, W.A. Goddard III., Chem. Phys. Lett. **3**, 414 (1969)
41. R.F. da Costa, F.J. da Paixao, M.A.P. Lima, J. Phys. B: At. Mol. Opt. Phys. **38**, 4363 (2005)
42. A.G. Falkowski, M.A.P. Lima, F. Kossoski, J. Chem. Phys. **152**, 244302 (2020)
43. M.A.P. Lima, T.L. Gibson, W.M. Huo, V. McKoy, Phys. Rev. A **32**, 2696 (1985)
44. M.A.P. Lima, T.L. Gibson, K. Takatsuka, V. McKoy, Phys. Rev. A **30**, 1741 (1984)
45. M.A.P. Lima, T.L. Gibson, K. Takatsuka, V. McKoy, Phys. Rev. A **30**, 3005 (1984)
46. R.F. da Costa, M.T.N. da Varella, M.H.F. Bettega, M.A.P. Lima, Eur. Phys. J. D **69**, 159 (2015)
47. Y. Kim, M.E. Rudd, Phys. Rev. A. **50**, 3954 (1994)
48. M.W. Schmidt, K.K. Baldridge, J.A. Boatz, S.T. Elbert, M.S. Gordon, J.H. Jensen, S. Koseki, N. Matsunaga, K.A. Nguyen, S.J. Su, T.L. Windus, M. Dupuis, J.A. Montgomery, J. Comput. Chem. **14**, 1347 (1993)
49. G.B. Bachelet, D.R. Hamann, M. Schlüter, Phys. Rev. B **26**, 4199 (1982)
50. M.H.F. Bettega, A.P.P. Natalense, M.A.P. Lima, L.G. Ferreira, Int. J. Quant. Chem. **60**, 821 (1996)
51. T.H. Dunning Jr., J. Chem. Phys. **53**, 2823 (1970)
52. See, for example, G.M. Moreira, M.H.F. Bettega, R.F. da Costa, J. Appl. Phys. **129**, 203301 (2021) and references therein
53. A. Osted, J. Kongsted, O. Christiansen, J. Phys. Chem. A **109**, 1430 (2005)
54. S. Iwata, K. Morokuma, Theor. Chimica Acta. **44**, 326 (1977)
55. D. Demoulin, Chem. Phys. **17**, 471 (1976)
56. T. Ari, M.H. Güven, J. Elec. Spec. Rel. Phenom. **106**, 29 (2000)
57. C. Fridh, J. Chem. Soc., Faraday Trans. 2 **74**, 190 (1978)
58. CRC *Handbook of Chemistry and Physics*, edited by D.R. Lide, 79th edn. (CRC, Boca Raton, 1998)